LBL-6732

THE SPECTROSCOPY OF NEW PARTICLES

Gerson Goldhaber

Department of Physics and Lawrence Berkeley Laboratory
University of California, Berkeley, California 94720

I. INTRODUCTION AND OUTLINE

Here I mean by "new" particles that I will limit myself to those hadrons containing one or more charmed quarks and to the anomalous eμ events as interpreted on the heavy lepton hypothesis. I will thus not review the recent evidence for baryon-antibaryon bound states. As we have learned from Leon Lederman's talk these are not all the new particles; he has presented clear-cut evidence for another "brand new" particle (or particles)! I refer to Lederman's talk at this conference for the details.

We can divide these newly discovered particles into six experimental categories.

The first three of these categories correspond to psion spectroscopy.

(i) Spin parity and charge conjugation, $J^{PC} = 1^{--}$; narrow states with $\sqrt{s} \leq 3.73$ GeV.

While there is nothing intrinsically special about $J^{PC} = 1^{--}$ versus some other quantum number of the $c\bar{c}$ state, it has had enormous experimental consequences. The fact that these vector mesons have the quantum numbers of the photon has been responsible for the opening up of the new physics. This allowed ψ production via the virtual photon of e^+e^- annihilation and similarly the discovery of the J because of the very characteristic signature of a high mass electron pair (or μ pair) which can be detected in an enormous background of other hadronic states.

(ii) $J^{PC} = 1^{--}$; broad states with $\sqrt{s} > 3.73$ GeV, the higher mass ψ particles. These are so far only observed in formation experiments via the virtual photon of e^+e^- annihilation.

(iii) $J^{PC} \neq 1^{--}$; narrow states, the X mesons. Here these states of positive charge conjugation have been reached via radiative decay from the ψ' and ψ. So far no corresponding broad states have been observed.

All these states are isosinglets and the evidence is now very good that they consist of a $c\bar{c}$ quark pair. They have "hidden charm" or the charm quantum number Ch = 0, and correspond to the charmonium spectrum.[1]

The next two categories correspond to charmed particles with Ch ≠ 0.

(iv) Charmed mesons with $Ch = \pm 1$. These consist of $c\bar{q}_i$ or $\bar{c}q_i$ where the index $i = 1,3$ goes over the "old" quarks u, d, s.

(v) Charmed baryons with $Ch = 1$. These consist of cq_iq_j where the indices $i,j = 1,3$ and their antiparticles. Here the charmed analogues of the Ξ and Ω^- can also exist, viz., ccq_i and ccc with $Ch = 2$ and 3 respectively. There is good evidence for $Ch = 1$ baryons and slight evidence for $Ch = 2$ baryons.

(vi) Anomalous eμ events and the Heavy Lepton Hypothesis.

II. PSION SPECTROSCOPY

The narrow states with the quantum numbers of the photon $J^{PC} = 1^{--}$

In November 1974 the whole picture of particle physics changed with the discovery of the ψ/J. Figure 1 illustrates the MIT-BNL discovery of the J, the SLAC-LBL discovery of the ψ and the rapid confirmation of both by the groups at Frascati. Figure 2 illustrates how at SPEAR within 10 days we switched to the "scanning mode" -- one point per MeV per minute. This mode showed the ψ clearly and shortly thereafter gave the ψ'. Figure 2 also shows the DESY confirmation of the ψ and ψ'. Then followed long months of search up to 7.7 GeV but no further narrow resonance with quantum numbers of the photon showed up! See Fig. 3.

The Breit-Wigner resonance expression for a final state channel a is:

$$\sigma_a = \frac{(2J+1)\pi}{E_{cm}^2} \frac{\Gamma_e \Gamma_a}{(E_{cm} - M_o)^2 + \frac{\Gamma^2}{4}} ,$$

where Γ, Γ_a, Γ_e are the total width, width for final state "a" and elastic width into an e^+e^- pair respectively. M_o is the resonance mass and $E_{cm} = 2E_o$ where E_o is the beam energy.

If $\Gamma/M_o \ll 1$, i.e., a very narrow resonance,

$$\int \sigma_a \, dE_{cm} = \frac{2\pi^2(2J+1)}{M_o^2} \frac{\Gamma_e \Gamma_a}{\Gamma}$$

and finally if $\Gamma_a = \Gamma_{hadronic} \approx \Gamma$ this integral becomes $\approx \frac{2\pi^2(2J+1)}{M_o^2} \Gamma_e$ and hence allows the determination of Γ_e. This expression -- after radiative corrections have been applied -- is essentially independent of ΔE, the beam spread. Values for $\int \sigma_{tot} dE$ are 11.4 μb MeV at the ψ/J, 3.4 μb MeV at the ψ' and the limits obtained in the 3.2 - 5.9 GeV region range from $< 0.6 - 0.9$ μb MeV while in the 5.9 - 7.7 GeV region they are < 0.45 μb GeV.

I will not repeat here the detailed studies of the decay properties and quantum numbers of the ψ and ψ' (see for example the review by Trilling[2]).

The broad levels with $J^{PC} = 1^{--}$

During 1975 two broad resonance states -- characteristic of decay into open channels -- in distinction to the narrow ψ and ψ' states whose decay is believed to be inhibited by the Okubo-Zweig-Iizuka rule[3] -- were discovered. A very broad state of $\Gamma \approx 200$ MeV centered at 4.1 GeV and a less broad state 4.414 GeV, $\Gamma = 33 \pm 10$ MeV. With more data the broad state gives strong indication of further substructure, but so far the full complexity of this energy region is not completely resolved. Figure 4 shows the entire data for $R = \sigma_{had}/\sigma_{\mu\mu}$ up to 7.7 GeV. The data on this figure comes from Novosibirsk, Orsay, Frascati, CEA and the SLAC-LBL experiment at SPEAR. In the 4 to 6 GeV regions there is good qualitative agreement as far as the resonance peaks are concerned between the SLAC-LBL data and that from DESY, both PLUTO and DASP, as presented at this conference by Timm. However there is a discrepancy by about 1 unit in R with the SLAC-LBL data giving the higher R values. This discrepancy lies within the systematic errors quoted by the various experiments. Here it must be remembered that the main systematic uncertainty comes from the Monte-Carlo calculations of the efficiencies. More new data will be needed to understand and resolve this discrepancy.

A brand new contribution presented at this conference by Litke comes from the "Lead Glass" addition to the SPEAR Mark I detector -- a LBL-SLAC-NWU-Hawaii collaboration.

Figure 5 shows this result: a new resonance at 3.772 GeV just above $D\bar{D}$ threshold and what is more the resonance decays principally into $D^0\bar{D}^0$ and D^+D^-. In Fig. 5a one notes the very pronounced radiative tail from the ψ'; in Fig. 5b all radiative effects have been subtracted and a fit to a Breit-Wigner resonance expression is given. A $^3D_1$ resonance had been predicted[4] at roughly this energy. A summary of the relevant resonance parameters is given in Table I. Figure 6 shows the 3.7 to 5 GeV region in detail.

The copious production of low momentum $D\bar{D}$ pairs at this resonance gives a new mass measurement of the D^0 and D^+ as will be discussed below.

The narrow states with $J^{PC} \neq 1^{--}$

There are four positive charge conjugation levels X observed which

TABLE I

Resonance parameters for the isolated ψ resonances. Γ is the full width, Γ_{ee} is the partial width to electron pairs, and B_{ee} is the branching fraction to electron pairs.

State	Mass[a] (MeV/c^2)	Γ (MeV/c^2)	Γ_{ee} (keV/c^2)	B_{ee}
ψ(3095)	3095	0.069 ± 0.015	4.8 ± 0.6	0.069 ± 0.009
ψ(3684)	3684 ± 5	0.228 ± 0.056	2.1 ± 0.3	$(9.3 \pm 1.6) \times 10^{-3}$
ψ(3772)	3772 ± 6	28 ± 5[b]	0.37 ± 0.09	$(1.3 \pm 0.2) \times 10^{-5}$
ψ(4414)	4414 ± 7	33 ± 10	0.44 ± 0.14	$(1.3 \pm 0.3) \times 10^{-5}$
ψ(4100)	~4100	~200 (unresolved)	~4	$\sim 2 \times 10^{-5}$

[a] Errors include a 0.13% uncertainty in the absolute energy calibration of SPEAR. The mass difference between the ψ(3684) and ψ(3772) is 88 ± 3 MeV/c^2. All masses are quoted relative to the ψ(3095) mass.

[b] Energy-dependent width evaluated at the mass of the resonance.

Table II. Branching fractions for $\psi' \to \gamma\gamma\psi$ and for inclusive γ rays. $B_\gamma = B(\psi' \to \gamma X_i)B(X_i \to \gamma\psi)$.

SLAC-LBL Data			MPPSSSD Data		
E_γ (MeV)[a]	B_γ (%)	$B(\psi' \to \gamma X_i)$ (%)	E_γ (MeV)	B_γ (%)	$B(\psi' \to \gamma X_i)$ (%)
343 ± 7	1.0 ± 0.6	--	361 ± 7	2.2 ± 1.0	7.0 ± 2
304 ± 5	2.4 ± 0.8	--	311 ± 7	5.0 ± 1.5	7.1 ± 1.9
254 ± 7	0.8 ± 0.4	--	--	--	--
113 ± 11	0.2 ± 0.2	7.5 ± 2.6[b]	113 ± 9	3.3 ± 1.7	7.2 ± 2.3[b]

[a] Resolution ~ 8 MeV.

[b] For a $1 + \cos^2\theta$ decay distribution.

are reached by radiative decay from the ψ'. There is one such state X(2830), observed at DESY only, which is reached by radiative decay from the ψ/J. The DASP experiment at DORIS observed a 4 s.d. peak $\psi/J \to \gamma X$, $X \to \gamma\gamma$ as reported by Timm at this conference.

There are three different types of information on the X states. These are:

(a) The reactions $\psi' \to \gamma_1\gamma_2\psi$, $\psi \to e^+e^-$ or $\mu^+\mu^-$

The reactions

$$\psi' \to \gamma_1 X_i \quad \Big|\to \gamma_2\psi$$

first observed at DORIS for $P_c \equiv X(3500)$, have been discussed by Timm at this conference. See also results in Table II.

(b) The inclusive γ spectra

The γ spectra has been studied by Whitaker et al.[5] in the SLAC-LBL Magnetic Detector at SPEAR and by Biddick et al.[5] in the Maryland-Princeton-Pavia-UC San Diego-SLAC-Stanford NaI detector in the east intersection region at SPEAR.

Whitaker et al. use γ conversion in the small amount of material, 0.05 radiation length, composed of the beam pipe and "pipe counters" near the center of the SLAC-LBL detector. Figure 7 shows the spectra at the ψ and ψ' as well as the γ-detection efficiency. One γ line $E_\gamma = 261 \pm 10$ MeV is observed at the ψ'. The results are given in Table II.

Biddick et al. use a detector shown in Fig. 8 consisting of large NaI scintillation counters as well as proportional wire chambers and proportional tube counters. The resulting γ-spectra for ψ and ψ' are shown in Fig. 9 and the results of a fit to the data are given in Table II. The agreement between the two experiments for $B(\psi' \to \gamma X(3415))$ is excellent. The comparison for $B_f = B(\psi' \to \gamma X)B(X \to \gamma\psi)$ however differs by as much as 2 s.d.

(c) The X → hadron decays

The hadronic X decay states are given in Fig. 10 from the SLAC-LBL data of Tanenbaum et al.[6] Here the final states have been fitted as 1C fits with a missing γ ray by application of the bubble chamber fitting program SQUAW to the SPEAR detector data. Tables III to V summarize these data and Tables VI from Vannucci et al.[7] and VII show some corresponding decays at the ψ/J and ψ' respectively.

From the fits to the hadronic final states we also get information on

Table III. $\chi(3415)$ branching ratios.

Decay Mode	Events	Efficiency	$B(\psi' \to \gamma\chi)\, B(\chi \to f)$	$B(\chi \to f)^a$
$\pi^+\pi^-$	32 ± 6	0.19	$(7.5 \pm 2.1) \times 10^{-4}$	$(1.0 \pm 0.3) \times 10^{-2}$
K^+K^-	27 ± 5.5	0.16	$(7.8 \pm 2.3) \times 10^{-4}$	$(1.0 \pm 0.3) \times 10^{-2}$
$\pi^+\pi^-\pi^+\pi^-$	181 ±16	0.19	$(3.5 \pm 0.7) \times 10^{-3}$	$(4.6 \pm 0.9) \times 10^{-2}$
$\pi^+\pi^-K^+K^-$	83 ±11	0.11	$(2.8 \pm 0.7) \times 10^{-3}$	$(3.7 \pm 0.9) \times 10^{-2}$
$\pi^+\pi^-p\bar{p}$	23 ± 6	0.18	$(4.7 \pm 1.3) \times 10^{-4}$	$(0.6 \pm 0.2) \times 10^{-2}$
$\pi^+\pi^-\pi^+\pi^-\pi^+\pi^-$	37 ± 8	0.08	$(1.4 \pm 0.5) \times 10^{-3}$	$(1.9 \pm 0.7) \times 10^{-2}$
$\psi\gamma$	1 ± 1	0.0011	$(2 \pm 2) \times 10^{-3}$	$(3 \pm 3) \times 10^{-2}$

[a] We use $B(\psi' \to \gamma\chi) = 0.073$ as obtained from Ref. 4. The errors quoted for $B(\chi \to f)$ do not include the overall scale uncertainty of 35% due to the error (± 0.0026) in $B(\psi' \to \gamma\chi)$.

Table IV. $\chi(3505)$ branching ratios.

Decay Mode	Events	Efficiency	$B(\psi' \to \gamma\chi)\, B(\chi \to f)$	$B(\chi \to f)^a$
$\pi^+\pi^-\pi^+\pi^-$	74 ± 12	0.20	$(1.4 \pm 0.4) \times 10^{-3}$	$(2.0 \pm 0.6) \times 10^{-2}$
$\pi^+\pi^-K^+K^-$	24 ± 7	0.11	$(0.8 \pm 0.3) \times 10^{-3}$	$(1.1 \pm 0.4) \times 10^{-2}$
$\pi^+\pi^-p\bar{p}$	6 ± 4	0.19	$(1.2 \pm 0.8) \times 10^{-4}$	$(1.7 \pm 1.1) \times 10^{-3}$
$\pi^+\pi^-\pi^+\pi^-\pi^+\pi^-$	48 ± 15	0.08	$(1.9 \pm 0.7) \times 10^{-3}$	$(2.7 \pm 1.1) \times 10^{-2}$
$\psi\gamma$	12 ± 4	0.0011	$(2.4 \pm 0.8) \times 10^{-2}$	$(34 \pm 11) \times 10^{-2}$

[a] We use $B(\psi' \to \gamma\chi) = 0.071$ from Ref. 5. The errors quoted for $B(\chi \to f)$ do not include the overall scale uncertainty of 27% due to the error (± 0.019) in $B(\psi' \to \gamma\chi)$.

Table V. $\chi(3550)$ branching ratios.

Decay Mode	Events	Efficiency	$B(\psi' \to \gamma\chi)\, B(\chi \to f)$	$B(\chi \to f)^a$
$\pi^+\pi^-$ or K^+K^-	9 ± 4	0.18	$(1.9 \pm 0.8) \times 10^{-4}$	$(2.7 \pm 1.1) \times 10^{-3}$
$\pi^+\pi^-\pi^+\pi^-$	89 ± 12	0.20	$(1.7 \pm 0.4) \times 10^{-3}$	$(2.4 \pm 0.6) \times 10^{-2}$
$\pi^+\pi^-K^+K^-$	47 ± 8	0.12	$(1.5 \pm 0.4) \times 10^{-3}$	$(2.1 \pm 0.6) \times 10^{-2}$
$\pi^+\pi^-p\bar{p}$	13 ± 5	0.19	$(2.6 \pm 1.0) \times 10^{-4}$	$(3.7 \pm 1.4) \times 10^{-3}$
$\pi^+\pi^-\pi^+\pi^-\pi^+\pi^-$	23 ± 15	0.08	$(0.9 \pm 0.6) \times 10^{-3}$	$(1.3 \pm 0.8) \times 10^{-2}$
$\psi\gamma$	4 ± 2	0.0009	$(1.0 \pm 0.6) \times 10^{-2}$	$(14 \pm 8) \times 10^{-2}$

[a] We use $B(\psi' \to \gamma\chi) = 0.070$ from Ref. 5. The errors quoted for $B(\chi \to f)$ do not include the overall scale uncertainty of 29% due to the error (± 0.020) in $B(\psi' \to \gamma\chi)$.

Table VI. Decay modes of the ψ into mesons.

Topology	Decay Mode	Observed Number of Events	Efficiency	Branching Ratio
K_SMM	$K_S K_L$	< 4	0.23	$<8.9 \times 10^{-5}$
$\pi^+\pi^-$	all	1.7 ± 1.7*	0.040	$(1.6 \pm 1.6) \times 10^{-4}$
K^+K^-	all	1.8 ± 1.4*	0.036	$(2.0 \pm 1.6) \times 10^{-4}$
$K_S K^\pm\pi^\mp$	all	126 ± 15	0.13	$(2.6 \pm 0.7) \times 10^{-3}$
	$K^0\bar{K}^{*0} + \bar{K}^0K^{*0}$	45 ± 7.8	0.044	$(2.7 \pm 0.6) \times 10^{-3}$
	$K^+K^{*-} + K^-K^{*+}$	48 ± 7.7	0.040	$(3.2 \pm 0.6) \times 10^{-3}$
	$K^0\bar{K}^{*0}\omega$, $\bar{K}^0K^{*0}\omega$	1 ± 2.7	0.007	$< 2.0 \times 10^{-3}$
	$K^+K^{*-} + K^-K^{*+}$	-1 ± 2.7	0.006	$< 1.5 \times 10^{-3}$
$\pi^+\pi^-K^+K^-$	all	205 ± 17	0.076	$(7.2 \pm 2.3) \times 10^{-3}$
	$K^{*0}\bar{K}^{*0}\omega$, $\bar{K}^{*0}K^{*0}\omega$	$40 \geq 8.4$	0.016	$(6.7 \pm 2.6) \times 10^{-3}$
	$K^{*0}\bar{K}^{*0}$	1.5 ± 4	0.048	$< 0.5 \times 10^{-3}$
	$K^{*0}\bar{K}^{*0}$	2.5 ± 4.5	0.009	$< 2.9 \times 10^{-3}$
	$\phi\pi^+\pi^-$	23 ± 5	0.043	$(1.4 \pm 0.6) \times 10^{-3}$
	ϕf	$\lesssim 1$	0.023	$< 3.7 \times 10^{-4}$
$\pi^+\pi^-\pi^+\pi^-K^+K^-$	all	30 ± 6	0.026	$(3.1 \pm 1.3) \times 10^{-3}$
	$\phi\pi^+\pi^-\pi^+\pi^-$	$\lesssim 3$	0.013	$\lesssim 1.5 \times 10^{-3}$
$K^+K^-K^+K^-$	all	19 ± 5	0.075	$(0.7 \pm 0.3) \times 10^{-3}$
	ϕK^+K^-	14 ± 5	0.040	$(0.9 \pm 0.4) \times 10^{-3}$
	$\phi f'$	6 ± 3	0.020	$(0.8 \pm 0.5) \times 10^{-3}$
$\pi^+\pi^-K^+K^-\pi^0$	all	309 ± 50	0.073	$(1.2 \pm 0.3) \times 10^{-2}$
	ωK^+K^-	22 ± 12	0.068	$(0.8 \pm 0.5) \times 10^{-3}$
	$\omega f'$	-2 ± 2.4	0.034	$< 1.6 \times 10^{-4}$
	$\phi\eta$	5 ± 2.5	0.013	$(1.0 \pm 0.6) \times 10^{-3}$
$\pi^+\pi^-K^+K^-$ MM	$\phi\eta'$	$\lesssim 2$	0.011	$\lesssim 1.3 \times 10^{-3}$
$2(\pi^+\pi^-)\pi^0$	all	675 ± 40*	0.17	$(4.0 \pm 1.0)\%$
	$\omega\pi^+\pi^-$	348 ± 40	0.14	$(6.8 \pm 1.9) \times 10^{-3}$
	ωf	81 ± 20	0.11	$(1.9 \pm 0.8) \times 10^{-3}$
	$\rho^0A_2^0 + \rho^\pm A_2^\mp$	36 ± 12	0.018	$(8.4 \pm 4.5) \times 10^{-3}$
$3(\pi^+\pi^-)\pi^0$	all	181 ± 26*	0.062	$(2.9 \pm 0.7)\%$
	$\omega 4\pi$	140 ± 30	0.044	$(8.5 \pm 3.4) \times 10^{-3}$
$4(\pi^+\pi^-)\pi^0$	all	13 ± 4*	0.014	$(9.0 \pm 3.0) \times 10^{-3}$
$\pi^+\pi^-\pi^0$	$(\rho^0\pi^0 + \rho^\pm\pi^\mp)$	153 ± 13*	0.12	$(1.3 \pm 0.3)\%$
$2(\pi^+\pi^-)$	all	76 ± 9*	0.19	$(4.0 \pm 1.0) \times 10^{-3}$
$3(\pi^+\pi^-)$	all	32 ± 7*	0.080	$(4.0 \pm 2.0) \times 10^{-3}$

Modes marked with an asterisk were calculated from a smaller data sample.

the decay angular distributions from which spin information can be derived. We can analyze the decay $\psi' \to \gamma X$ in terms of $\frac{d\sigma}{d\cos\theta} \sim 1 + a\cos^2\theta$ where θ is the angle at which the γ is emitted relative to the incident positron direction. Then for $J(X) = 0$ we get a unique prediction $a = 1$. For $J(X) = 1$ and 2 the predictions are not unique but assuming only a dipole amplitude gives $a = -0.33$ and $a = 0.08$ respectively. See Table VIII for the experimental values of a.

Furthermore one can also study the decay

$$X \to \gamma\psi$$
$$\quad\; \downarrow \to \ell^+\ell^-$$

where now the γ direction is taken relative to the ℓ^+ direction. Here the same angular distributions obtain for the same assumptions as above. Finally one can use the full angular correlations in the cascade:

$$\psi' \to \gamma_1 X \;,\; X \to \gamma_2 \psi \;,\; \psi \to \ell^+\ell^-$$

as discussed in detail in Tanenbaum et al.[6] The current status on the spin-parity of the X states is summarized in Table VIII and Fig. 11.

Residual problems

As discussed by Jackson at this conference if we accept the X(2830) and X(3450) as the η_c and η_c' respectively, the large splittings and the observed radiative rates are hard to understand. Also there is the problem why are there no hadronic decay modes observed for these objects? In the case of the X(2830) one could argue that hadronic decay modes could be hidden among the enormous background of hadronic decays from the ψ involving a missing π^o. However at the X(3450) within the present statistics no evidence of a hadronic is observed. Both these subjects will require more data.

Finally there is another state predicted, the $^1P_1$, $J^{PC} = 1^{+-}$ negative charge conjugation state which cannot be reached by radiative decay from the ψ' and hence has not been observed as yet.

III. CHARMED PARTICLES

The properties of charmed mesons

There is by now very little doubt that the new narrow resonances at 1865 MeV/c^2 which decay into strange final states are the D^o and D^+ predicted by charm theory.

There are five new items regarding charmed mesons:

Table VII. $\psi'(3684)$ branching ratios into all charged hadrons.

Decay Mode	Events	Efficiency	$B(\psi' \to f)$[a]
$\pi^+\pi^-\pi^+\pi^-$	49 ± 9	0.20	$(0.45 \pm 0.1) \times 10^{-3}$
$\pi^+\pi^-K^+K^-$	53 ± 8	0.12	$(0.8 \pm 0.2) \times 10^{-3}$ to $(1.6 \pm 0.4) \times 10^{-3}$
$\pi^+\pi^-p\bar{p}$	41 ± 7	0.19	$(0.4 \pm 0.1) \times 10^{-3}$ to $(0.8 \pm 0.2) \times 10^{-3}$
$\pi^+\pi^-\pi^+\pi^-\pi^+\pi^-$	9 ± 5	0.08	$(0.15 \pm 0.1) \times 10^{-3}$

[a]The ψ' branching ratios have been corrected in order to remove the nonresonant background. For $\psi' \to \pi\pi KK$ and $\psi' \to \pi\pi p\bar{p}$, which can also proceed by strong decay, the nonresonant background cannot be uniquely determined from our data. The smaller (larger) value for the branching ratio applies if the decay is entirely electromagnetic (strong).

Table VIII. Summary of X Spin-Parity Information.

State and Mass	Information Source: $\pi^+\pi^-/K^+K^-$ Final State	Photon Angular Distribution in Hadronic Decays	Cascade Angular Correlations	Suggested J^P
X(3415) 3414 ± 3 MeV	$J^P = 0^+, 2^+$..	consistent with $J = 0$ $a = 1.4 \pm 0.4$	—	0^+
X(3505) 3503 ± 4 MeV	$J^P \neq 0^+, 2^+$.. suggested	$J \neq 0$ (2σ level) $a = 0.1 \pm 0.4$	$J \neq 0$ (5σ level)	1^+
X(3550) 3551 ± 4 MeV	$J^P = 0^+, 2^+$..	$J \neq 0$ (2σ level) $a = 0.3 \pm 0.4$	—	2^+
X(3455) 3454 ± 7 MeV	No Information			

(a) σ·B determinations at 4.03 and 4.41 GeV

At 4.03 and 4.41 GeV, the main peaks in R, we have taken extended runs in the SLAC-LBL detector at SPEAR; namely, integrated luminosities of 1.3 and 1.6 pb^{-1} respectively.

As shown in Piccolo et al.[8] we have identified clear cut mass peaks for the decay modes:

$$D^0 \to K^-\pi^+ \quad (1)$$
$$\to K^0\pi^+\pi^- \quad (2)$$
$$\to K^-\pi^+\pi^-\pi^+ \quad (3)$$
$$D^+ \to K^-\pi^+\pi^+ \quad (4)$$

(and the corresponding charge conjugate states). In addition Litke in his talk at this conference showed clear evidence for the further decay mode

$$D^+ \to K^0_S\pi^+ \quad (5)$$

Figure 12 shows the invariant mass distributions for reactions (1-4) at the two E_{cm} values studied. As all D's are produced in associate production with a $\bar{D}$, $\bar{D}^*$ or more complex state including a $\bar{D}$ we have applied a cut on the recoil system at 1.8 GeV. This does not lose any signal but improves the signal-to-background ratio. Figure 13 shows the invariant mass distribution for $\pi^+\pi^-$, K^+K^-, $\pi^+\pi^-\pi^\pm$, $K^\pm\pi^+\pi^-$, $K^+K^-\pi^\pm$ and $K_S\pi^\pm$ final states at 4.03 GeV. The first two final states show kinematic reflections of the 1865 $K^-\pi^+$ mass peak due to deficiencies in time-of-flight identification of kaons and pions. In addition these two final states correspond to Cabbibo suppressed decays and limits can be set on these. The expected rates are $\Gamma(D^0 \to \pi^+\pi^-)/\Gamma(D^0 \to K^-\pi^+) = \tan^2\theta_c \cong 0.05$ while $D^0 \to K^+K^-$ is doubly suppressed ($\cong 0.0025$). For both these decay mode ratios we find 90% CL upper limits of 0.07. All measured σB values are summarized in Table IX.

Finally we searched for K^* and ρ^0 production in the final states. Only the decay mode (3) shows evidence for such a resonance. Assuming that the $K3\pi$ signal is the sum of the four decays, direct $K3\pi$, $K^{*0}\pi^+\pi^-$, $K^\mp\pi^\pm\rho^0$, $K^{*0}\rho^0$, we unfold the signal fractions by comparison with the Monte-Carlo calculation for each mode. The results of the fit are summarized below:

Phase Space	$K^\mp\pi^\pm\rho^0$	$K^*\pi^+\pi^-$	$K^*\rho^0$
$0.05^{+0.11}_{-0.05}$	$0.85^{+0.11}_{-0.22}$	$0.00^{+0.2}_{-0.0}$	$0.10^{+0.11}_{-0.10}$

Table IX. Event populations, efficiencies and values of σB for several D^0, $\bar{D}^0$ and D^+, D^- decay modes.

Decay Mode	c.m. Energy (GeV)	No. of Events	Detection Efficiency	Cross Section × Branching Ratio σB (nb)
$K^-\pi^+$	4.03	182 ± 18	0.25 ± 0.04	0.57 ± 0.11
$\bar{K}^0\pi^+\pi^- + K^0\pi^+\pi^-$		61 ± 14	0.044 ± 0.007	1.09 ± 0.30
$K^-\pi^+\pi^+\pi^-$		95 ± 23	0.09 ± 0.02	0.83 ± 0.27
$K^-\pi^+\pi^+$		82 ± 14	0.16 ± 0.03	0.40 ± 0.10
$\bar{K}^0\pi^+ + K^0\pi^+$		9.5 ± 6.5	0.07 ± 0.01	< 0.18
$\pi^-\pi^+$		$5.4 \pm {}^{8.8}_{4.5}$	0.27 ± 0.04	< 0.04
K^-K^+		$5.2 \pm {}^{7.5}_{5.2}$	0.24 ± 0.04	< 0.04
$\pi^-\pi^+\pi^+$		$0.0 \pm {}^{8.0}_{0.0}$	0.22 ± 0.03	< 0.03
$\pi^-K^+K^-$		$2.7 \pm {}^{7.1}_{2.7}$	0.13 ± 0.03	< 0.06
$K^-\pi^+\pi^-$		$0.0 \pm {}^{4.7}_{0.0}$	0.16 ± 0.03	< 0.02
$K^+\pi^-$	4.41	92 ± 18	0.19 ± 0.04	0.30 ± 0.09
$\bar{K}^0\pi^+\pi^- + K^0\pi^+\pi^-$		55 ± 14	0.037 ± 0.010	0.91 ± 0.34
$K^-\pi^+\pi^+\pi^-$		119 ± 41	0.08 ± 0.02	0.91 ± 0.39
$K^-\pi^+\pi^+$		67 ± 19	0.125 ± 0.03	0.33 ± 0.12

Remarkably enough, there is no significant K^* production whereas $K^{\mp}\pi^{\pm}\rho^0$ seems to be the dominant mode. This is illustrated in Fig. 14. We find no evidence of A_2, and set a 90% confidence level upper limit of 0.06 for the ratio of $K^{\mp}A_2^{\pm}$ to total $K3\pi$.

(b) Inclusive K^0 production

The inclusive K^0 cross section is measured through the $K_S^0 \to \pi^+\pi^-$ decay mode. The important question here is to obtain a pure K_S^0 sample. The details of K^0 selection are given in the paper by Lüth et al.[9] Figure 15 shows the result of K^0 selection which include a cut on the angle ξ between the K^0 direction and the line from the origin to the vertex of the K^0. A demand of a minimum and maximum vertex distance of 1 and 16 cm respectively, a cut on the opening angle of the vee with an acceptance interval from 10° to 170°, and more. Figure 15 shows the resulting $\pi^+\pi^-$ invariant mass spectrum at two incident energies, 4.03 and 7.3-7.6 GeV. Finally, Fig. 15 also shows the proper time distribution of the K^0 candidates. The straight lines correspond to the accepted K_S^0 lifetime. Figure 16 shows the ratio $f_K = 2\sigma_{K_S}/\sigma_{Had}$. This can be interpreted as the fraction of events with a neutral K; the assumption is made that the number of K_S and K_L are equal. As may be noted at 4.03 and 4.41 there is a distinct enhancement in f_K. Figure 16b shows R_K defined as $R_K = 2\sigma_{K_S}/\sigma_{\mu\mu}$. This thus corresponds to the ratio of the neutral K cross section to the μ pair cross section. Here one can observe the peaks at 4.03 and 4.41 very distinctly. In addition one notes a general increase from a level of about 1 in the 3.6 GeV region to about 2 beyond the onset of the charm threshold. The results from DORIS (DASP) shown by Timm are very similar except that they do not observe the peak at 4.41. The reason for this is apparently that the DESY group did not have an extensive run just at the peak of this resonance. Thus their points near 4.41 are averages over a much wider energy region. Figure 17 shows $s d\sigma/dx$ for the K_S^0 production. In Fig. 17a we note a comparison of the data at 4.03 and the 3.4-4 GeV region. We note that beyond $X = 0.5$ the two distributions are consistent. However at low X values there is a distinct excess in the 4.03 resonance region which we know is dominated by charm production. In Fig. 17b the energies 4.03 and 4.41 are compared with the high energy 6.8-7.6 GeV. Here again beyond $X = 0.5$ or 0.6 the distributions are consistent, suggesting scaling. However the strong excess at low X are noted both for 4.03 and 4.41 GeV. The excess in the low X region is very similar to that shown

already at the 1975 photon conference by Schwitters for all charged particles combined. A simple interpretation of this excess comes from the fact that charmed mesons are produced in pairs and thus the secondaries from each D, which again has to decay into at least two particles, are limited to X values less than 0.5.

(c) Study of the recoil system against D

In Fig. 18c we show the (background subtracted) recoil mass distribution against a D^o where here all the data samples are added together. Thus in this figure we have a highly non-uniform integrated luminosity distribution from E_{cm} = 3.9 - 4.6 GeV. Of the four prominent structures, the second and third peaks come largely from the 4.028 GeV data. We observe narrow peaks in M_{recoil} at $\cong$ 1860 MeV/c^2, $\cong$ 2005 MeV/c^2, $\cong$ 2145 MeV/c^2 and a broader peak at $\cong$ 2440 MeV/c^2. We interpret the first three peaks as follows[10]:

$$e^+e^- \rightarrow D^o\bar{D}^o \qquad (6)$$

$$e^+e^- \rightarrow D^o\bar{D}^{*o} \text{ and } \bar{D}^oD^{*o} \qquad (7)$$

$$e^+e^- \rightarrow D^{*o}\bar{D}^{*o} \ . \qquad (8)$$

A priori, an alternate possibility exists for the third peak; viz., $e^+e^- \rightarrow D^o\bar{D}^{*o}$ and charge conjugate. This interpretation however can be ruled out, as can be noted from Fig. 18a and b. The curves in this figure are calculated on the basis of reaction (8). We observe a clearcut shift and broadening of the peak at $\sim$ 2145 MeV/c^2 (E_{cm} = 4.028) to $\sim$ 2200 MeV/c^2 (E_{cm} = 4.415). The enhancement at 2440 MeV/c^2 and width $\Gamma \cong$ 100 MeV/c^2 could be due to multibody processes such as $D^*\bar{D}^*\pi$, for example or, alternatively, production of a charmed state of higher mass.

In a corresponding M_{recoil} distribution for the exotic channel $K^{\mp}\pi^{\pm}\pi^{\pm}$, the background is more severe and the data is of a lower statistical significance (signal $\sim$ 160 events). We observe a prominent peak at $M_{recoil} \sim$ 2010 MeV/c^2 which can be interpreted as

$$e^+e^- \rightarrow D^+D^{*-} \text{ and charge conjugate} \ . \qquad (9)$$

Also indications for the presence of the other three peaks observed in the recoil spectrum against the D^o. In particular there is evidence for

$$e^+e^- \rightarrow D^{*+}D^{*-} \ , \qquad (10)$$

only weaker relative to reaction (9).

D* decay modes

The possible charm conserving D^* decay modes are:

$D^{*0} \rightarrow \gamma D^0$ observed (11)

$D^{*0} \rightarrow \pi^0 D^0$ observed (12)

$D^{*0} \rightarrow \pi^- D^+$ kinematically forbidden (13)

$D^{*+} \rightarrow \gamma D^+$ (14)

$D^{*+} \rightarrow \pi^0 D^+$ one or both observed (15)

$D^{*+} \rightarrow \pi^+ D^0$ observed (16)

To study the $D^{*+} \rightarrow \pi^+ D^0$ decay mode we have examined the $E_{cm} = 5.0 - 7.8$ GeV region where for high D^{*+} momenta the decay π^+ becomes readily detected, as discussed in Feldman et al.[11] In Fig. 19 we show the $K^\mp \pi^\pm$ mass distribution for D^0 momenta > 1.5 GeV/c. We note a clear although somewhat broader D^0 peak. We then select $K\pi$ combinations in the D^0 signal (1820 - 1910 MeV/c^2) and compute the $D^0\pi^\pm$ mass combinations. The quantity that is precisely measured is the mass difference $M(D^0\pi) - M(D^0)$. This mass difference is plotted in Fig. 20. From this data we find the $D^{*+} - D^0$ mass difference to be 145.3 ± 0.5 MeV/c^2 or equivalently the Q value for decay mode (16) is 5.7 ± 0.5 MeV. We use this information as a constraint in the mass determinations below. The observed width of the peak in Fig. 20a is consistent with the expected resolution from Monte-Carlo calculations. Thus $\Gamma(D^{*+}) < 2$ MeV/c^2. This implies that even though we are dealing with a strong charm conserving decay, because of the small Q value for p wave pion decay Γ is rather small.

Masses and relative production rates

For mass determination we focus on a single energy: $E_{cm} = 4.028$ GeV. We can then consider momentum distributions p of the two-particle system. In Fig. 21b we show the momentum spectrum for the two-body decays of the D^0, in 10 MeV intervals. In Fig. 21c the same for the $K^\mp\pi^\pm\pi^\pm$ system. Figure 21a illustrates the various processes contributing to the D^0 spectrum.

We note three distinct contributions to the peak corresponding to $D^{*}\bar{D}^{*}$ production, process (8), depending on the source of the observed D^0's. It is clear that the shape of the corresponding peak is a sensitive function of whether we are dealing with π^0 or γ decay of D^{*0}. For π^0 decay we get a Gaussian distribution while for γ decay we get a distribution with $dN/dp^2 =$ constant or $dN/dp \propto p$, which results in a triangular shape. Finally for D^0 production from the D^{*+} feed-down decay mode, process (16), we expect a separate peak. As there is no evidence for such a peak this means that either the D^{*0} and D^{*+} masses are nearly degenerate, or the rate of contributions from process (16) is low. The value of the D^* mass, for

process (12) or (16), is a sensitive function of p_3; viz., $dM(D^*) \cong -0.1\, dp_3$.

The second peak and its associated shoulder is due to $D\bar{D}^*$ (and charge conjugate) production, process (7). Here as we note from Fig. 21a there are four contributing processes. The central value of p_2 determines $M_D + M_{D^*}$, while the shape of the shoulder and peak determine the relative contributions of the four processes. Finally the third "peak" (which appears clearly in a 20 MeV/c binning) is due to $D\bar{D}$ production, process (6). A similar -- though simpler -- situation holds for the D^+ spectrum.

We have fitted this data under two separate sets of assumptions: the normal fit and the isospin constrained fit. The detailed description of the assumptions are given in Goldhaber et al.[10] The data were fit under both sets of assumptions with various starting points, background functions, and resolutions in order to study the stability of the results. Some parameters vary outside of statistical errors depending on the type of fit.

To get a feeling for these two types of fits in columns 2 and 3 of Table X we show average values obtained from a number of different versions of these fits, while in column 4 of the Table we present the parameters we judge to be most reliably determined along with our estimate of their total uncertainty including systematic errors. The solid curves of Figs. 21b and 21c show the results of a typical fit of the second type.

We note from Table X that the relative importance of reactions (6), (7), (8) for the D^o, D^{*o} channels can be expressed as:

$$D^o\bar{D}^o : D^o\bar{D}^{*o} + \bar{D}^oD^{*o} : D^{*o}\bar{D}^{*o}$$

$$0.2 \pm 0.1 : \quad 4.0 \pm 0.8 \quad : 128 \pm 40$$

where a p^3 phase space factor has been explicitly removed. These ratios are to be compared with the spin counting estimates[4,12] of 1:4:7, which are in strong disagreement with the data. Various explanations of this behavior have been discussed in the literature.

Table X shows the best mass values obtained from the above fits. At this conference Litke reported improved mass values for the D^o and D^+ from the data at $\psi(3772)$. I am here and in Fig. 22 quoting the latest update of these masses as reported by Feldman at the SLAC Topical Conference in July 1977.

$$M(D^o) = 1863.3 \pm 0.9 \text{ MeV/c}^2$$
$$M(D^+) = 1868.4 \pm 0.9 \text{ MeV/c}^2$$

Table X. Results from simultaneous fits to the D^0, D^+ momentum spectra at E_{cm} = 4.028 GeV.

	Fit parameter	Normal fit	Isospin constrained fit	Estimated values
Masses in MeV/c^2	M_{D^0}	1864 (1.5)[a]	1862 (0.5)[a]	1863 ± 3[b]
	M_{D^+}	1874 (2.5)	1873 (2.0)	1874 ± 5
	$M_{D^{*0}}$	2006 (0.5)	2007 (0.5)	2006 ± 1.5
	$M_{D^{*+}}$	2009 (1.5)	2007 (0.5)	2008 ± 3
Branching ratios	$BR(D^{*0} \to \gamma D^0)$	0.45 (0.08)	0.75 (0.05)	0.55 ± 0.15
	$BR(D^{*+} \to \pi^+ D^0)$[c]	--	0.60 ± 0.15	--
	$\frac{BR(D^+ \to K^- \pi^+ \pi^+)}{BR(D^0 \to K^- \pi^+)}$[c]	--	1.60 ± 0.60	--
D^0 source fractions	$D^0\bar{D}^0$	0.05 (0.03)	0.05 (0.02)	0.05 ± 0.03
	$D^0\bar{D}^{*0} + \bar{D}^0 D^{*0}$	0.42 (0.04)	0.34 (0.04)	0.38 ± 0.08
	$D^{*0}\bar{D}^{*0}$	0.47 (0.05)	0.32 (0.05)	0.40 ± 0.10
	$D^{*+}D^-$, $D^{*+} \to \pi^+ D^0$	0.03 (0.02)	0.09 (0.04)	0.06 ± 0.05
	$D^{*+}D^{*-}$, $D^{*+} \to \pi^+ D^0$	0.03 (0.03)	0.20 (0.07)	0.11 ± 0.10
D^+ source fractions	D^+D^-	0.09 (0.05)	0.09 (0.05)	0.09 ± 0.05
	$D^{*+}D^- + D^{*-}D^+$	0.65 (0.07)	0.58 (0.06)	0.62 ± 0.09
	$D^{*+}D^{*-}$	0.26 (0.08)	0.33 (0.08)	0.29 ± 0.10

[a] Quantities in parentheses are typical statistical errors for a single fit.

[b] Errors quoted include estimated systematic uncertainty.

[c] These values can only be obtained under the assumptions of the isospin constrained fit. The quoted errors do not reflect possible breakdown of these assumptions.

$$M(D^{*0}) = 2006 \pm 1.5 \text{ MeV}/c^2$$
$$M(D^{*+}) = 2008.6 \pm 1.0 \text{ MeV}/c^2 .$$

(d) $D^0 - \bar{D}^0$ mixing

We have obtained two independent results related to the question of $D^0 - \bar{D}^0$ mixing. In the $E_{cm} = 3.9 - 4.6$ GeV data we have established an upper limit on charm events exhibiting apparent strangeness violation; i.e., events where the kaon observed in the recoil system has the same charge as the kaon found in the D^0. We find that less than 18% of events containing a D^0 exhibit an apparent strangeness violation (90% CL).[10]

It has been suggested[13] that the presence of first-order $|\Delta C| = 2$ neutral currents would create $D^0 - \bar{D}^0$ mixing on time scales considerably shorter than the D^0 lifetime. If this were true, nearly 1/2 of events containing a D^0 would exhibit strangeness nonconservation. Our results clearly rule this out.

In the $E_{cm} = 5 - 7.8$ GeV data[11] we have tested whether the decay proceeds as:

$$D^{*+} \rightarrow \pi^+ D^0$$
$$\qquad\qquad\quad \hookrightarrow K^-\pi^+ \qquad \text{(exotic final state)}$$

as expected for no $D^0 - \bar{D}^0$ mixing, or as:

$$D^{*+} \rightarrow \pi^+ \bar{D}^0$$
$$\qquad\qquad\quad \hookrightarrow K^+\pi^- \qquad \text{(nonexotic final state)} .$$

At the 90% confidence level, the fraction of the time that a D^0 decays as if it were a $\bar{D}^0$ (e.g., to $K^+\pi^-$ instead of $K^-\pi^+$) is less than 16%. The relationship between these two measurements depends in detail on the D^0 production mechanism[14] over the full energy range from 3.9 to 4.6 GeV, which is unknown at present.

(e) Measurements on the spin of the D^0 and D^{*0}

Nguyen et al.[15] have shown that for D^0 and D^{*0} spin values less than 2 the best values are 0 and 1 as expected from charm theory.

Charmed baryons

The evidence for charmed baryons[16] was reviewed at this conference by a member of the Columbia-FNAL-Illinois group.

IV. THE HEAVY LEPTON HYPOTHESIS

The anomalous e-μ events

The presence and properties of the e-μ events, first observed by Perl et al.[17] in the SLAC-LBL experiment at SPEAR, are now confirmed in three

independent experiments. The two experiments at DORIS PLUTO and DASP as discussed in Timm's talk and the Lead Glass Wall experiment which gives an improved e identification as discussed in Litke's talk.

One new feature given in Perl et al.[18] is the detailed study of the phenomenological eμ cross section. At the peaks for charm production of 4.03 and 4.41 GeV no increase in the eμ cross section is observed, showing clearly that different phenomena are involved.

In view of the already mentioned talks at this conference I will not discuss any further details here except to mention that the Heavy Lepton Hypothesis appears to be the most likely interpretation of the phenomenon.

I wish to thank Ms. Christina Frank for her meticulous work in typing and compiling this report.

This work was supported by the U. S. Energy Research and Development Administration.

REFERENCES

1. T. Appelquist et al., Phys. Rev. Lett. 34, 365 (1975); E. Eichten et al., Phys. Rev. Lett. 34, 369 (1975).
2. G. H. Trilling, Proceedings of the SLAC Summer Institute on Particle Physics (1975) and LBL-4276.
3. S. Okubo, Phys. Lett. 5, 105 (1963); G. Zweig, CERN Report Th-401, 412 (1964), unpublished; J. Iizuka, K. Okada and O. Shito, Prog. Theor. Phys. 35, 1061 (1966).
4. K. Lane and E. Eichten, Phys. Rev. Lett. 37, 477 (1976).
5. J. S. Whitaker et al., Phys. Rev. Lett. 37, 1596 (1976) and C. J. Biddick et al., Phys. Rev. Lett. 38, 1324 (1977).
6. M. Tannenbaum et al., submitted to Phys. Rev. D.
7. F. Vannucci et al., Phys. Rev. 15D, 1814 (1977).
8. M. Piccolo et al., Phys. Lett. B (to be published).
9. V. Lüth et al., Phys. Lett. B (to be published).
10. G. Goldhaber et al., Phys. Lett. B (to be published).
11. G. Feldman et al., Phys. Rev. Lett. 38, 1313 (1977).
12. A. De Rujula, H. Georgi, and S. L. Glashow, Phys. Rev. Lett. 37, 398 (1976).
13. See for example, S. L. Glashow and S. Weinberg, Phys. Rev. D15, 1958 (1977) and E. A. Paschos, Phys. Rev. D15, 1966 (1977).
14. R. L. Kingsley, Phys. Lett. 63B, 329 (1976).

15. H. K. Nguyen et al., Phys. Rev. Lett. 39, 262 (1977).
16. E. G. Cazzoli et al., Phys. Rev. Lett. 34, 1125 (1975), B. Knapp et al., Phys. Rev. Lett. 37, 882 (1976).
17. M. L. Perl et al., Phys. Rev. Lett. 35, 1489 (1975).
18. M. L. Perl et al., Phys. Lett. B (to be published).

NOV 1974

MIT - BNL

J

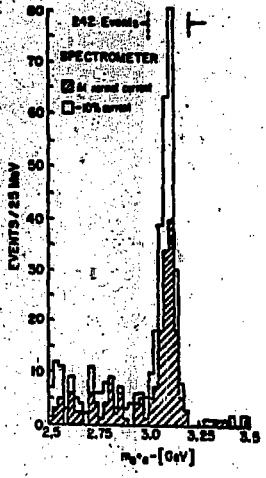

SLAC - LBL

ψ

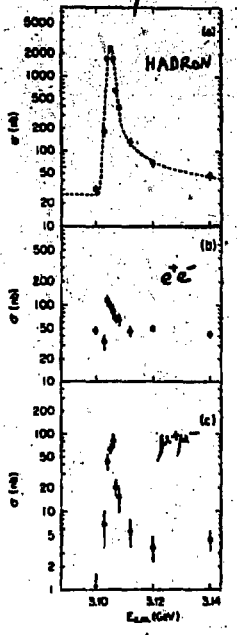

FRASCATI

ψ/J

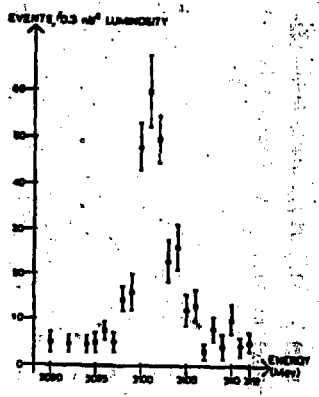

Fig. 1. ψ/J history.

XBL 7510-8476

SLAC-LBL NOV 74

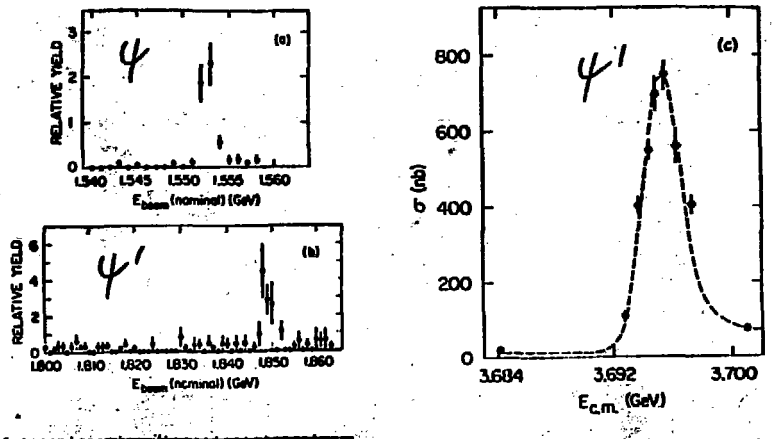

XBL 7510-8467

Fig. 2. ψ' history.

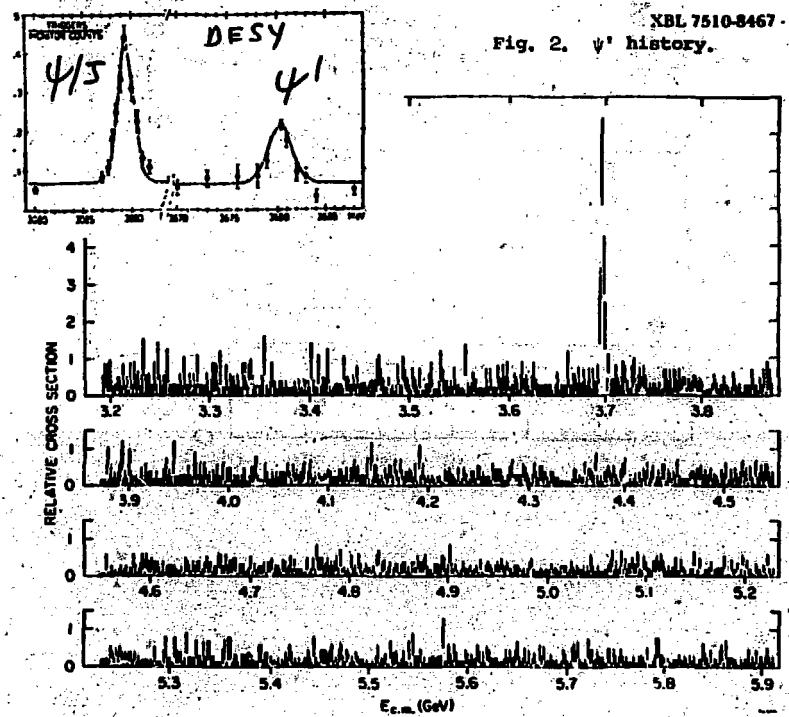

Fig. 3. Total hadronic cross section vs E_{cm} in fine steps over the range 3.2 GeV ≤ E_{cm} ≤ 5.9 GeV. The clear peak is the ψ(3684). Similar data were taken up to 7.6 GeV.

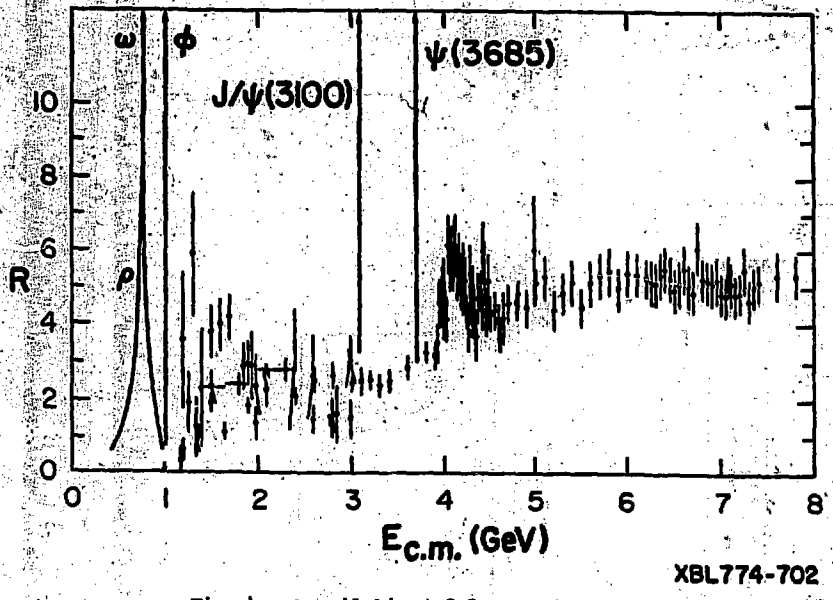

Fig. 4. Compilation of data on R.

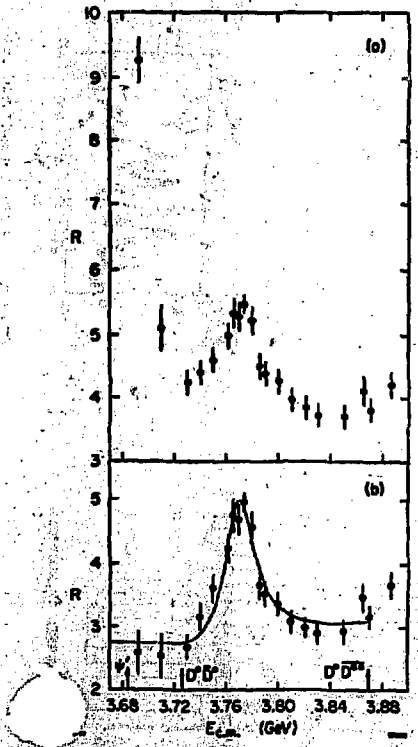

Fig. 5. The new Lead Glass Wall results from SPEAR. The $\psi(3772)$ (a) no radiative corrections, (b) with radiative correction; curve corresponds to fit of Breit-Wigner expression.

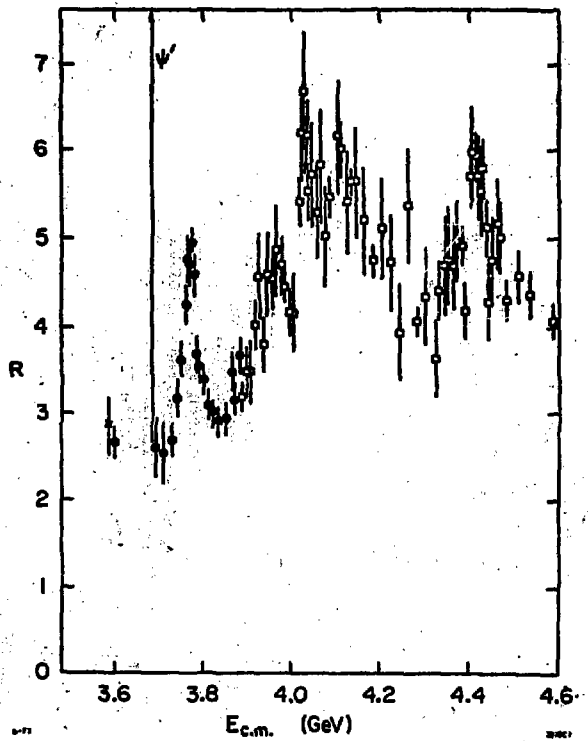

Fig. 6. Details of the region 3.6-4.6 with $\psi'(3684)$ subtracted.

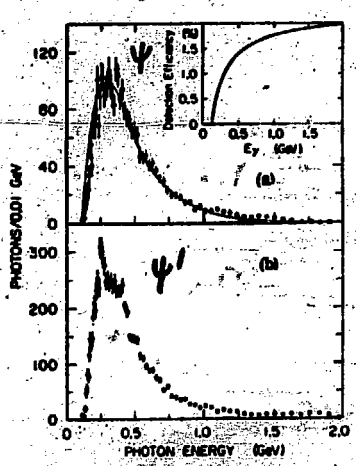

Fig. 7. Photon spectrum from SLAC-LBL experiment at SPEAR. Fitted values for ψ' decay are given in Table II.

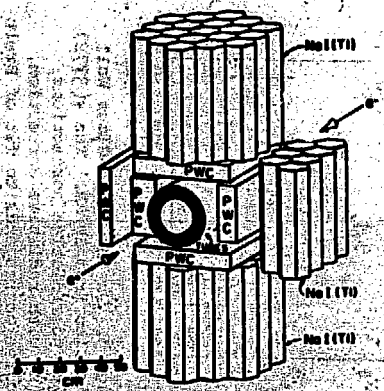

Fig. 8. The MPPSSSD apparatus at SPEAR.

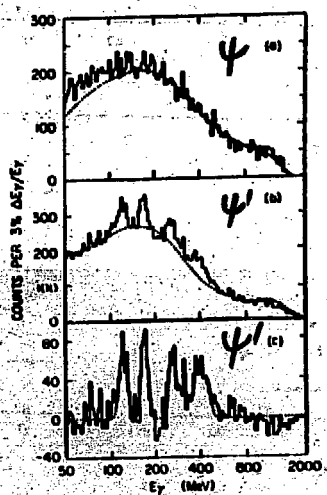

Fig. 9. Photon spectrum from MPPSSSD experiment at SPEAR. Fitted values for ψ' decay are given in Table II.

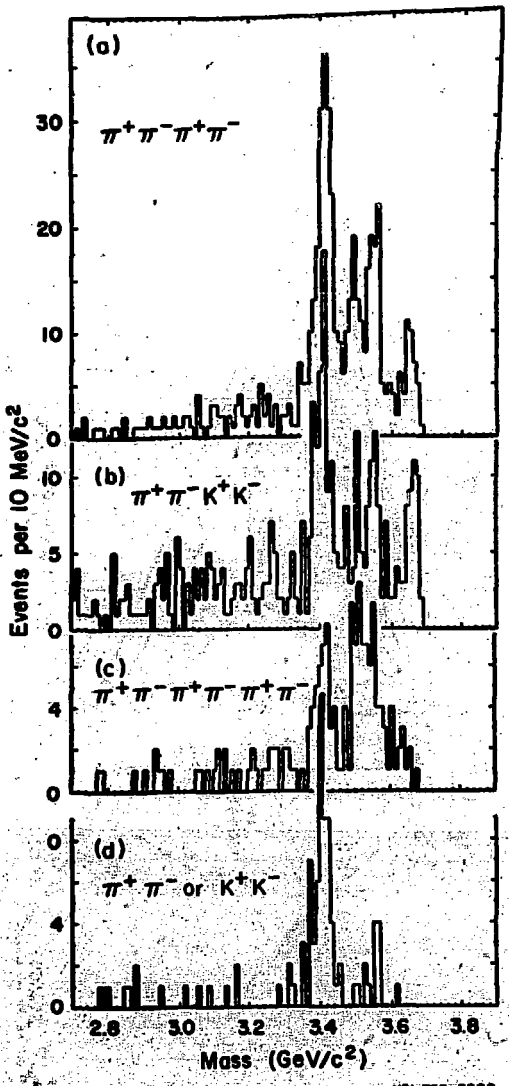

Fig. 10. Mass spectrum for multihadron states X fit to the reaction $\psi' \to \gamma X$ with X being (a) $\pi^+\pi^-\pi^+\pi^-$, (b) $\pi^+\pi^-K^+K^-$, (c) $\pi^+\pi^-\pi^+\pi^-\pi^+\pi^-$, (d) $\pi^+\pi^-$ or K^+K^-.

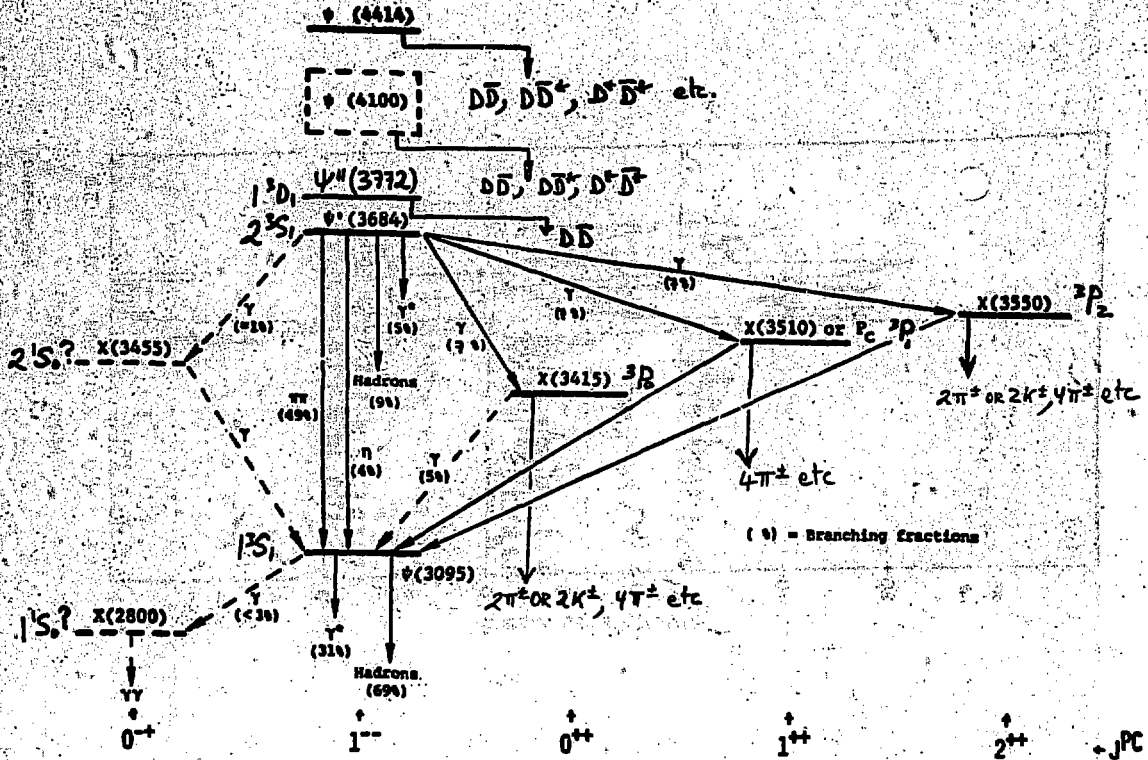

Fig. 11. Current status of psion spectroscopy.

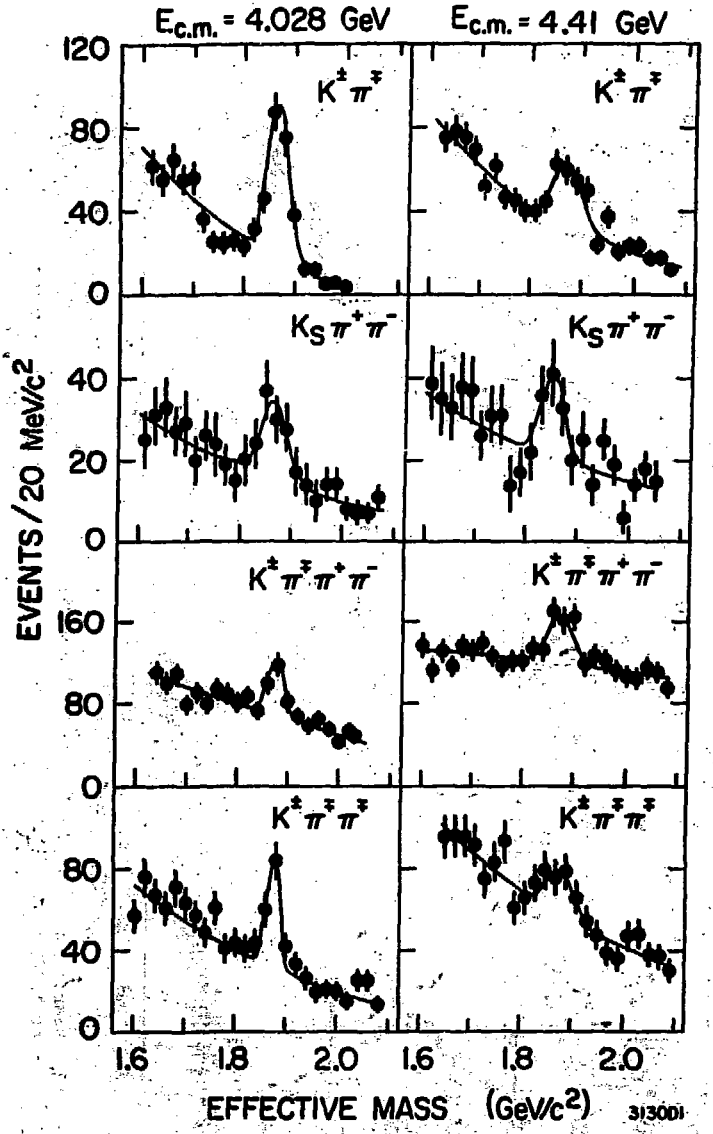

Fig. 12. D^0, D^+ production at 4.028 and 4.41 GeV. SLAC-LBL experiment at SPEAR.

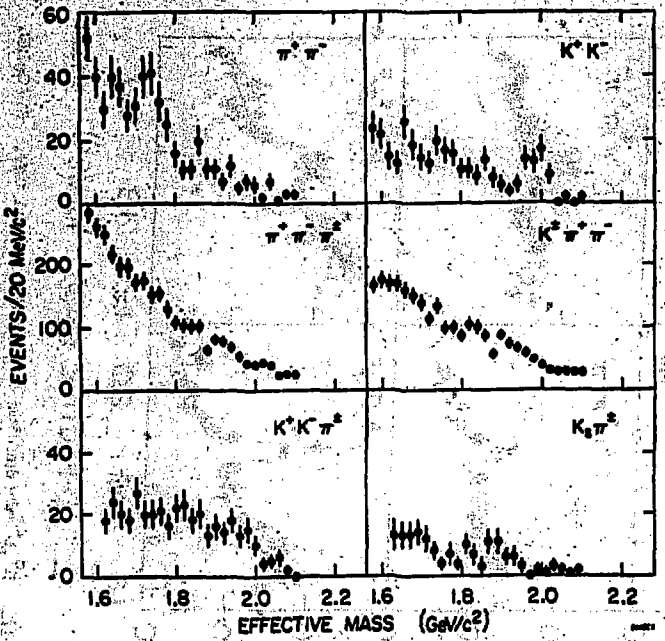

Fig. 13. Search for D^0, D^+ Cabibbo forbidden decay modes at 4.028 GeV.

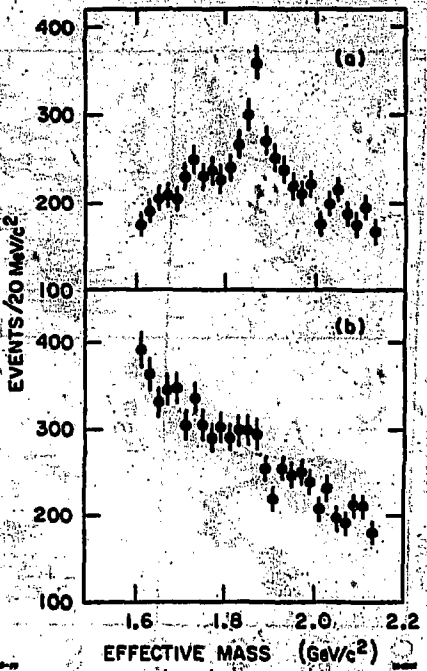

Fig. 14. $K^-\pi^+\pi^-\pi^+$ production at (a) ρ^0 band selected, (b) ρ^0 band excluded.

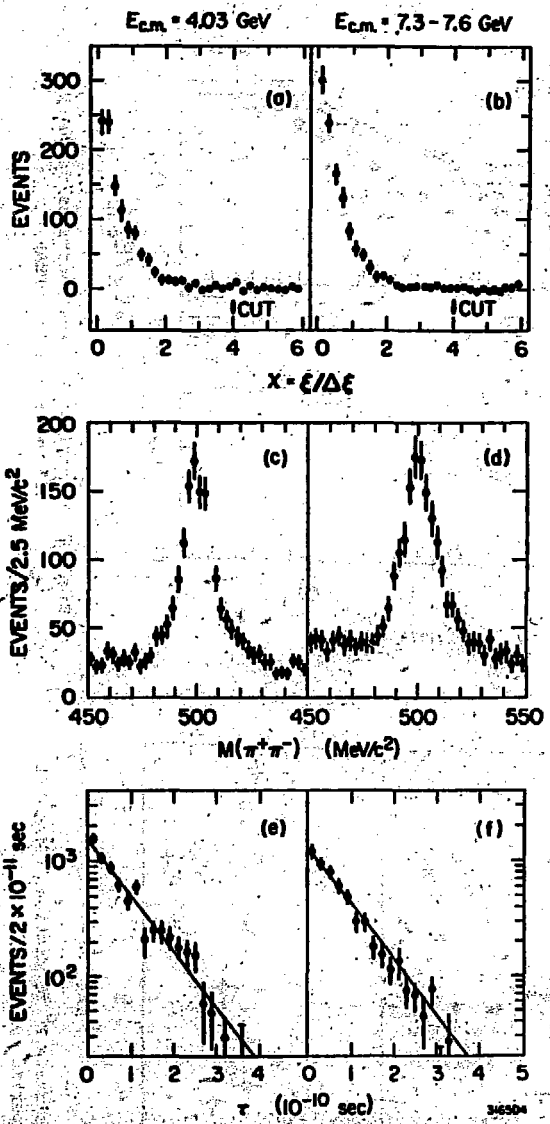

Fig. 15. (a) and (b) angle ξ described in text. (c) and (d) $K^0_S \to \pi^+\pi^-$ signal. (e) and (f) proper time distributions for observed K^0_S.

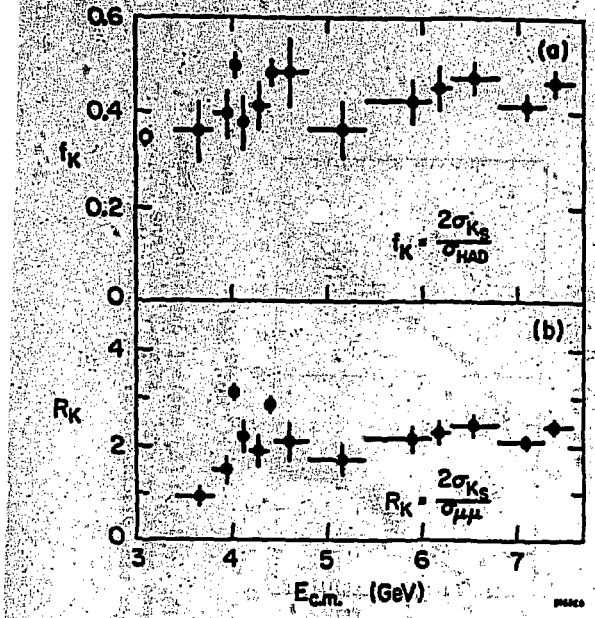

Fig. 16. Inclusive K^0 production. SLAC-LBL experiment at SPEAR.

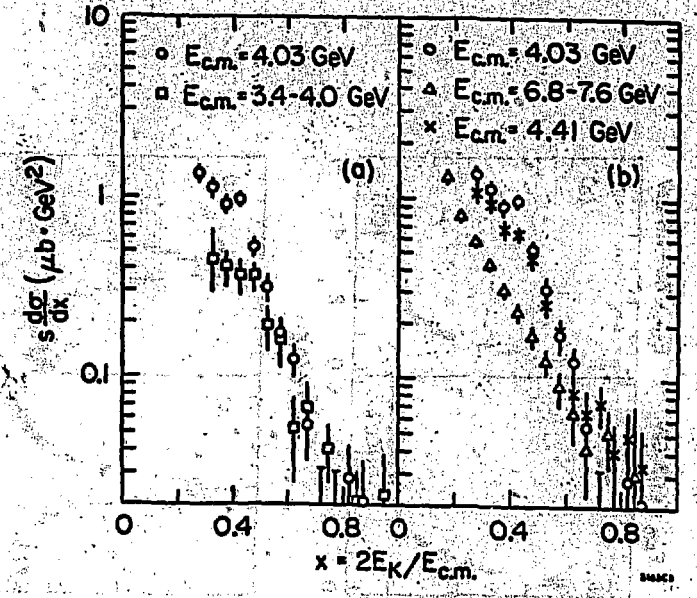

Fig. 17. Invariant K^0 cross sections versus x. SLAC-LBL experiment at SPEAR.

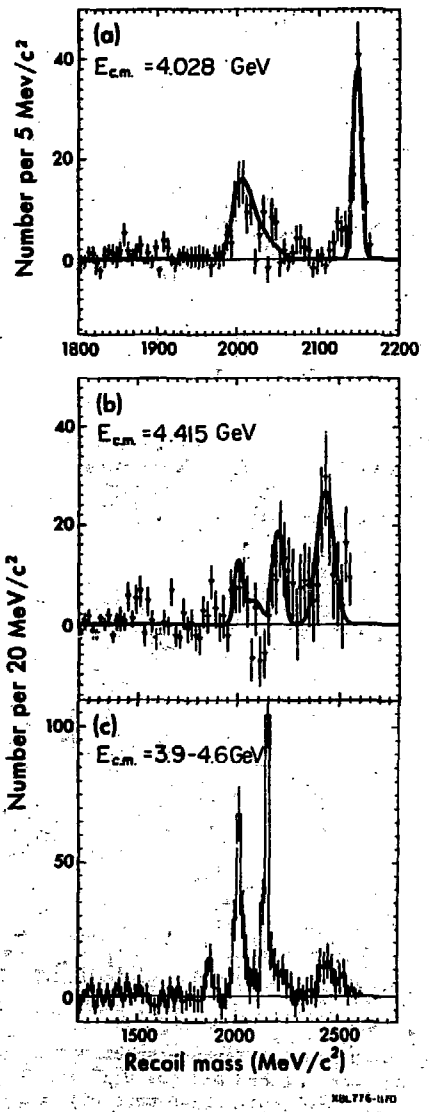

Fig. 18. Recoil spectra against D^0.

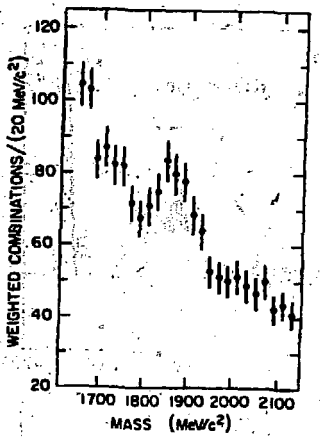

Fig. 19. Weighted invariant-mass spectrum for $K^{\pm}\pi^{\mp}$ combinations with momenta greater than 1.5 GeV/c at $\langle E_{cm} \rangle = 6.8$ GeV.

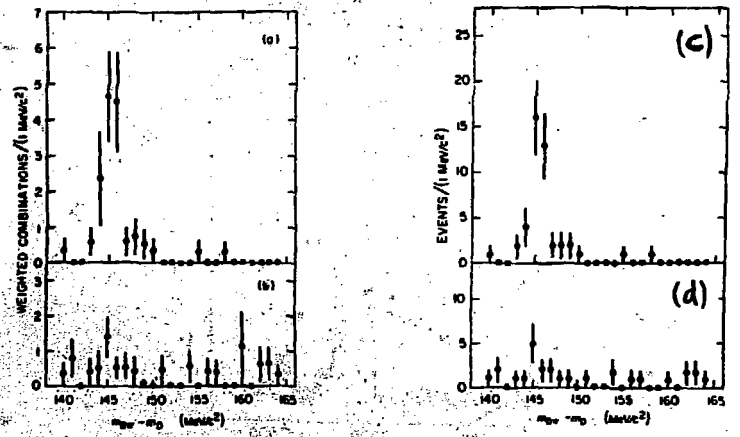

Fig. 20. Weighted Dπ-D mass difference spectra for (a) $D^0\pi^+$ and $\bar{D}^0\pi^-$ (i.e., $K^{\mp}\pi^{\pm}\pi^{\pm}$) combinations and (b) $\bar{D}^0\pi^+$ and $D^0\pi^-$ (i.e., $K^{\mp}\pi^{\pm}\pi^{\mp}$) combinations. Unweighted Dπ-D mass difference spectra for (c) $D^0\pi^+$ and $\bar{D}^0\pi^-$ (i.e., $K^{\mp}\pi^{\pm}\pi^{\pm}$) combinations and (d). $\bar{D}^0\pi^+$ and $D^0\pi^-$ (i.e., $K^{\mp}\pi^{\pm}\pi^{\mp}$) combinations.

Fig. 21. (a) Illustrative example of the contributions to the expected D^0 momentum spectrum near threshold:

$e^+e^- \rightarrow D^{*+}D^{*-}$,	$D^{*+} \rightarrow \pi^+D^0$		(A)
$\rightarrow D^{*0}\bar{D}^{*0}$,	$D^{*0} \rightarrow \pi^0D^0$		(B)
$\rightarrow D^{*0}\bar{D}^{*0}$,	$D^{*0} \rightarrow \gamma D^0$		(C)
$\rightarrow D^{*+}D^-$,	$D^{*+} \rightarrow \pi^+D^0$		(D)
$\rightarrow D^{*0}\bar{D}^0$,	$D^{*0} \rightarrow \pi^0D^0$		(E)
$\rightarrow \bar{D}^{*0}D^0$	direct D^0		(F)
$\rightarrow D^{*0}\bar{D}^0$,	$D^{*0} \rightarrow \gamma D^0$		(G)
$\rightarrow D^0\bar{D}^0$	direct D^0		(H)

(b) $D^0 \rightarrow K^-\pi^+$ momentum spectrum at $E_{cm} = 4.028$ GeV. The solid curve is a typical fit described in text. (c) $D^+ \rightarrow K^-\pi^+\pi^+$ momentum spectrum at $E_{cm} = 4.028$ GeV compared to a typical fit. The dashed curve corresponds to background.

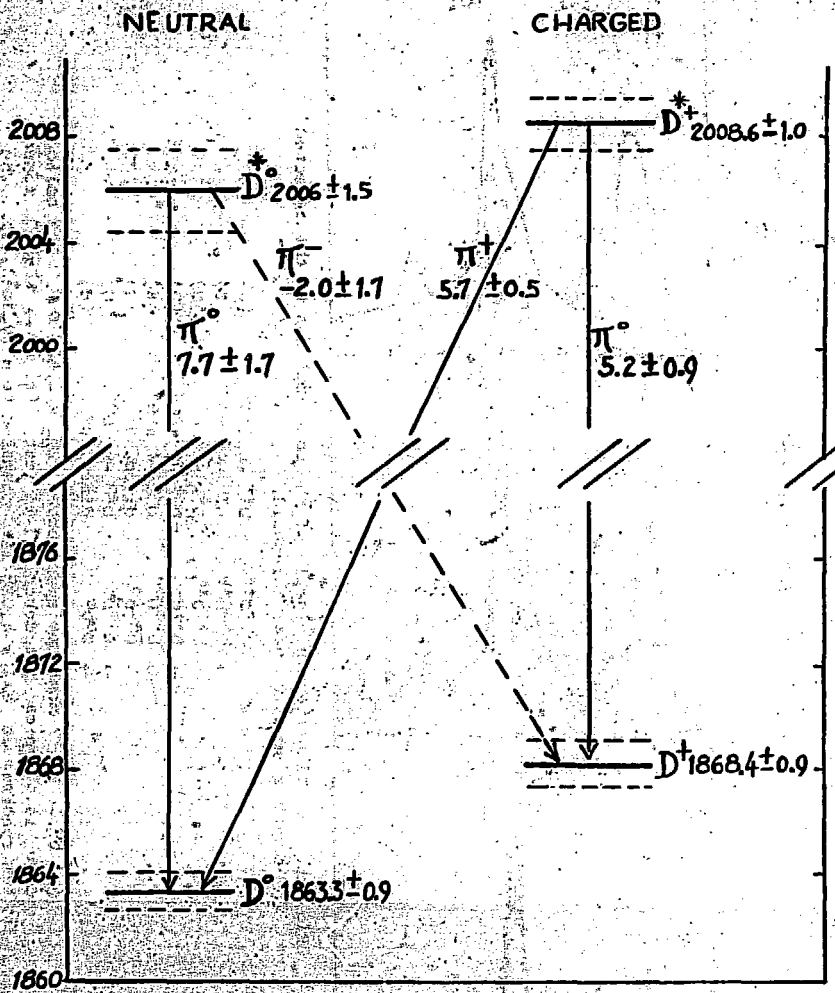

Fig. 22. D, D* mass values and pion transitions.